technologies

Article

A Novel Approach to Quantitative Characterization and Visualization of Color Fading

Woo Sik Yoo [1,2,*], Kitaek Kang [1], Jung Gon Kim [1] and Yeongsik Yoo [3,*]

1 WaferMasters, Inc., Dublin, CA 94568, USA; kitaek.kang@wafermasters.com (K.K.); junggon.kim@wafermasters.com (J.G.K.)
2 Institute of Humanities Studies, Kyungpook National University, Daegu 41566, Republic of Korea
3 College of Liberal Arts, Dankook University, Yongin 16890, Republic of Korea
* Correspondence: woosik.yoo@wafermasters.com (W.S.Y.); ysyoophd@dankook.ac.kr (Y.Y.)

Abstract: Color fading naturally occurs with time under light illumination. It is triggered by the high photon energy of light. The rate of color fading and darkening depends on the substance, lighting condition, and storage conditions. Color fading is only observed after some time has passed. The current color of objects of interest can only be compared with old photographs or the observer's perception at the time of reference. Color fading and color darkening rates between two or more points in time in the past can only be determined using photographic images from the past. For objective characterization of color difference between two or more different times, quantification of color in either digital or printed photographs is required. A newly developed image analysis and comparison software (PicMan) has been used for color quantification and pixel-by-pixel color difference mapping in this study. Images of two copies of Japanese wood-block prints with and without color fading have been selected for the exemplary study of quantitative characterization of color fading and color darkening. The fading occurred during a long period of exposure to light. Pixel-by-pixel, line-by-line, and area-by-area comparisons of color fading and darkening between two images were very effective in quantifying color change and visualization of the phenomena. RGB, HSV, CIE L*a*b* values between images and their differences of a single pixel to areas of interest in any shape can be quantified. Color fading and darkening analysis results were presented in numerical, graphical, and image formats for completeness. All formats have their own advantages and disadvantages over the other formats in terms of data size, complexity, readability, and communication among parties of interest. This paper demonstrates various display options for color analysis, a summary of color fading, or color difference among images of interest for practical artistic, cultural heritage conservation, and museum applications. Color simulation for various moments in time was proposed and demonstrated by interpolation or extrapolation of color change between images, with and without color fading, using PicMan. The degree of color fading and color darkening over the various moments in time (past and future) can be simulated and visualized for decision-making in public display, storage, and restoration planning.

Keywords: color fading; color quantification; color difference; image analysis; statistical analysis; software; pixel-by-pixel color difference mapping

check for updates

Citation: Yoo, W.S.; Kang, K.; Kim, J.G.; Yoo, Y. A Novel Approach to Quantitative Characterization and Visualization of Color Fading. *Technologies* **2023**, *11*, 108. https://doi.org/10.3390/technologies11040108

Academic Editor: Pietro Zanuttigh

Received: 12 July 2023
Revised: 1 August 2023
Accepted: 4 August 2023
Published: 8 August 2023

1. Introduction

The energy of photons has the potential to cause irreversible damage to objects [1–3]. The photon energy increases with the shortening of wavelength. For the visible wavelength range of 380–700 nm (violet to red), the photon energy corresponds to 3.26–1.77 eV [4]. The higher energy side of photons, from blue to ultraviolet (UV) light, can be especially deleterious to colorants, resulting in visible fading [5]. Conservators understand that light-sensitive objects have a finite life for display under illumination. Most collecting institutions often adopt guidelines to indicate the lighting conditions and duration of exhibitions based on the characteristics of substances and art media such as oil paintings, watercolors, metal sculptures, and so on. These guidelines assume that objects within a class share a similar known stability under the same illumination conditions. Some of those assumptions have been brought into question, and additional investigations use a micro fading tester (MFT) to predict a colorant's rate of fade over time [6].

The MFT is an analytical technique proposed and developed by Paul Whitmore of Carnegie Mellon University to determine the in situ light sensitivity of a piece of artwork [6,7]. The MFT was designed to rapidly induce and monitor color change in small areas of fugitive materials. This is achieved by exposing the sample surface to a stable, high-intensity focused light spot (typically 0.5 mm or less in diameter) and simultaneously examining the affected area using a spectrophotometer. The resulting color change may be perceived as photo-induced damage from the small area of exposure to very intense light. Once a minimum color change threshold is reached, even if the change is visually imperceptible, the test is terminated. The MFT allows the direct identification of the most fugitive colorants in an artwork by comparing the color change behavior of other colorants and light-sensitive standard materials. This predictive information for specific colorants used in an artwork is very valuable when deciding on a preservation lighting policy [1,7]. Characterization of color fading and its rate determination as a function of aging conditions are of strong interest in the fields of art, museum, cultural heritage, paint, fabrics, food, plant, materials, and so on [8–16].

There is a well-documented European Standard on the Conservation of cultural property—Test methods—Colour measurement of surfaces [17]. It describes a test method to measure the surface color of porous inorganic materials and their possible chromatic changes. However, no reference to the appearance of glossy surfaces is described. The method may be applied to porous inorganic materials either untreated or subjected to any treatment or aging. The method is suitable for the measurement of color coordinates of representative surfaces of objects, indoors or outdoors, and representative surfaces of specimens described in the document.

In this paper, we propose a novel approach to quantitative characterization visualization of color fading and color darkening by image comparisons using image analysis/processing software (PicMan) capable of color analysis from single pixels, lines, and areas of any shape and size up to the entire image. We demonstrate various display options for color analysis comparisons of color fading or color difference among images of interest for practical applications in the field of art, cultural heritage, and museums. Potential applications of color interpolation between images and the possibility of extrapolation beyond referenced images for predicting future color appearance simulation are discussed.

2. Images and Analysis Methods

2.1. Test Images

Two copies of a Japanese woodblock print by Utamaro used in a Microfading Workshop given in 2014 were selected as test images [1,18]. Figure 1 shows the two copies of the Japanese woodblock print by Utamaro (a) before and (b) after light exposure to cause significant color fading. According to the source, they were identical twins when they were printed. They were made from the same materials and printed in the same way. They were probably printed by the same people. Then the two copies were separated after printing, with one image experiencing significant color fading by light exposure. The light exposure has caused profound changes to a majority of colors used in the print. Some colors, such as the blue on the kimono (Japanese dress), are not very light-sensitive compared to the other colors. The purpose of the microfading experiment at the Getty workshop was to gain information on the light sensitivity of each colorant without the identical twins as a reference. Assuming the images were used as an example in a Microfading Workshop for professionals in the field, the images were digitized using the same equipment under the same conditions, including lighting conditions and environment.

(**a**) (**b**)

Figure 1. Two identical copies of a Japanese woodblock print by Utamaro before and after significant light exposure [17]: (**a**) as printed; (**b**) after light exposure.

2.2. *Image Analysis/Processing Software (PicMan)*

Image processing and analysis are very different from image editing (brightening, straightening, white balancing, contrast stretching, resizing, etc.) or image modification using commercially available software such as Photoshop, Illustrator, or Lightroom, as well as many other photo-editing software. More than one type of software is required to efficiently perform desired tasks on digital photographs, images, videos, and documents. Multiple image-editing application software requires tremendous data processing power and memory as resources. They are operating on PCs simultaneously in the background to perform very specific tasks of varying complexity. The demand for computing resources is increasing exponentially with the increase in the number of files and size of image files. The development of integrated image analysis/processing software suitable for frequently needed image editing, processing, and various analysis functions with image, video, and numerical data exporting capabilities is strongly desired. Ideally, all desired tasks should be able to be performed from a regular PC with reasonable computing power and without opening multiple applications and switching between applications.

As reported previously, the authors' group has been developing user-friendly software (PicMan, WaferMasters, Inc. Dublin, CA, USA) for image-based dimension (length, area, circumference, circularity, etc.) measurement/analysis, quantitative color analysis, statistical analysis, and various image-tailoring functions to address the deficiencies in the above-mentioned areas with existing software [19–21]. Pattern selection, area selection, highlighting, editing, coloring, and transparency application to any digital image can be easily done. A few applications of these functions have been successfully applied to archaeology, cultural heritage, conservation science, material science, biology, medical science, semiconductor research, and development studies [21–25]. PicMan can handle various formats of digital image and video files such as JPG, BMP, GIF, PNG, TGA, TIFF, WEBP, JPEG XR, PDF, CR2, DM3, ND2, MIRAX, MOV, MP4, AVI, WMV, etc. for image analysis and processing. Detailed application examples of PicMan can be found in previous reports from other study groups [19–25]. Several new functions, such as pixel-by-pixel color difference mapping, block comparison, color interpolation, and extrapolation, for color fading characterization, have been added to this study.

All digital images have a set of pixel information on the x and y coordinates and RGB brightness. Combinations of RGB brightness values at different coordinates determine the color, brightness, and shapes of interest. Combining the RGB brightness (8 bits per channel), values can generate more than 16 million colors (2^8 = 256 brightness values $\times$ 3 channels = $2^8 \times 3$ colors = 224 colors = 16,777,216 colors) in displays and monitor screens. However, it is more difficult to understand how we feel, recognize, and interpret colors and shapes from visual stimulation. The differences in the spectral intensity distribution of light (wavelength dependence of brightness in the visible wavelength range of 380–700 nm, 400–700 nm, or 400–780 nm) make us perceive corresponding colors. In the course of color model and theory development, many different concept customs of color spaces have been introduced to characterize and classify colors in quantitative and traceable manners suitable for the field of applications.

The most popular color spaces used across disciplines are RGB, HSV, CIE L*a*b*, and Munsell models. The RGB and CIE L*a*b* color spaces are built on cartesian coordinates, while the HSV and Munsell color spaces are based on cylindrical coordinates. The CIE L*a*b* coordinate is based on RGYB instead of RGB. The CIE L* value indicates lightness assuming grayscale, while the a* and b* values are determined by the balance between red–green and yellow–blue, respectively. For conversion between RGB and CIE L*a*b* color spaces, a new cartesian coordinate of XYZ is introduced to add Y (yellow) color component into account [20,25–27]. Then, the XYZ values were used for L*a*b* values in the CIE L*a*b* color spaces. All digital images are based on combinations of RGB channel brightness. The color information in the other color spaces can be calculated from the RGB values. Details of color space transformations and color conversion in different color spaces can be found elsewhere [25–27]. All 16,777,216 colors are assigned six-digit hexadecimal color codes for computer graphics. The capability of pixel-by-pixel color extraction, and the average color extraction of selected areas, can be very useful for quantitative color characterization for a variety of applications. All colors can be quantified as numerical values or corresponding hexadecimal color codes. It is extremely helpful for objective communication and reproduction of colors, hue, tint, tone, and shade.

3. Results

Color quantification and comparisons between the two images before and after color fading (shown in Figure 1) were made point-by-point, line-by-line, area-by-area, and block-by-block. Color information was extracted and exported as data files in CSV format for further analysis. Details of color characterization, statistical analysis, and comparison results are described in the following subsections.

3.1. Histogram Analysis

Figure 2 shows a screenshot image of image analysis software (PicMan) for color information extraction at 34 points of five-pixel diameter regions of interest (ROIs) and a 284 $\times$ 422 pixel (=119,848 pixels) rectangle (white border line) area per printed image. The selected rectangular ROIs are the identical location on individual images. RGB and L*a*b* histogram analysis was done for the rectangle (white border line) areas of the two images to gain insight into the overall color distribution and lightness values. Then, the identical 34 points were selected for point-by-point color comparison and color information extraction for further analysis.

The RGB and CIE L*a*b* histograms of two rectangle areas with white border lines on the images before and after color fading and color darkening (in Figure 2) were plotted in Figure 3a–d. The image before color fading showed wide RGB intensity distribution due to the vibrant colors of the print image, as shown in Figure 3a. The CIE L*a*b* histogram showed a high CIE L* value peak at around 78, corresponding to bright colors on the image. As seen in Figure 3b, the majority of colors show a slightly reddish color (i.e., low positive value for CIE a*) and mild yellowish color (i.e., low positive values for CIE b*). The presence of small portions of pixels with a greenish color component can be recognized from the small area under negative CIE a* values in the range of −5 to 0.

Figure 2. A screenshot image of image analysis software (PicMan) for color information extraction at 34 points of five-pixel diameter regions of interest (ROIs) and a 284 × 422 pixel (= 119,848 pixels) rectangle (white border line) area per print. For easy comparisons, different colors for the numbers of ROIs for two images were used.

The RGB and CIE L*a*b* histograms of the print after color fading were also plotted in the same vertical and horizontal scales for easy comparison (Figure 3c,d). The red peak became stronger, and small peaks below 192 became flatter, showing the brightening of the print after color fading (and darkening) after light exposure. The increase of RGB intensity and the loss of variation in RGB histogram are the results of discoloration and detailed pattern loss in print. The CIE L*a*b* histogram also showed a very sharp and intense positive CIE a* peak between 5–10 and a broadening of the positive side of the CIE b* histogram graph extending toward the higher positive CIE b* values toward yellowish color after color fading. These agree well with the RGB histogram and the effect of color fading.

As seen in Figure 3, a decrease of 'frequency (number of pixels with a given brightness in RGB channel)' and broadening of the green and blue channel histogram and the opposite trends of the green channel histogram are noticed after color fading or darkening of certain colors. Similar trends in L*a*b* color space (i.e., some values increased, others decreased) are observed. Most colors became lighter (color fading), and some became darker (color darkening) with light exposure. It should be noted that the pixels with the L* value in the range of 40–70 before color fading have increased their L* value to 60–74 after color fading. It is a good indicator for color fading in most printed areas by light exposure.

Table 1 shows the RGB and CIE L*a*b* statistics of a rectangle area before and after color fading (and darkening). As seen from the table, the average values of RGB increased while the standard deviation of RGB intensity decreased after color fading. The average color change between the two test images before and after color fading/darkening can be easily judged in L*, a*, b*, and RGB values. It clearly indicates that the color became brighter, and details are lost after color fading. The CIE L*a*b* statistics showed an increase in the average CIE L* value and a decrease in CIE a* and CIE b* values. This can be interpreted that most colors were lightened and approached natural tone colors. The standard deviations of the CIE L*a*b* values were decreased after color fading, a clear indicator of the loss of contrast after color fading.

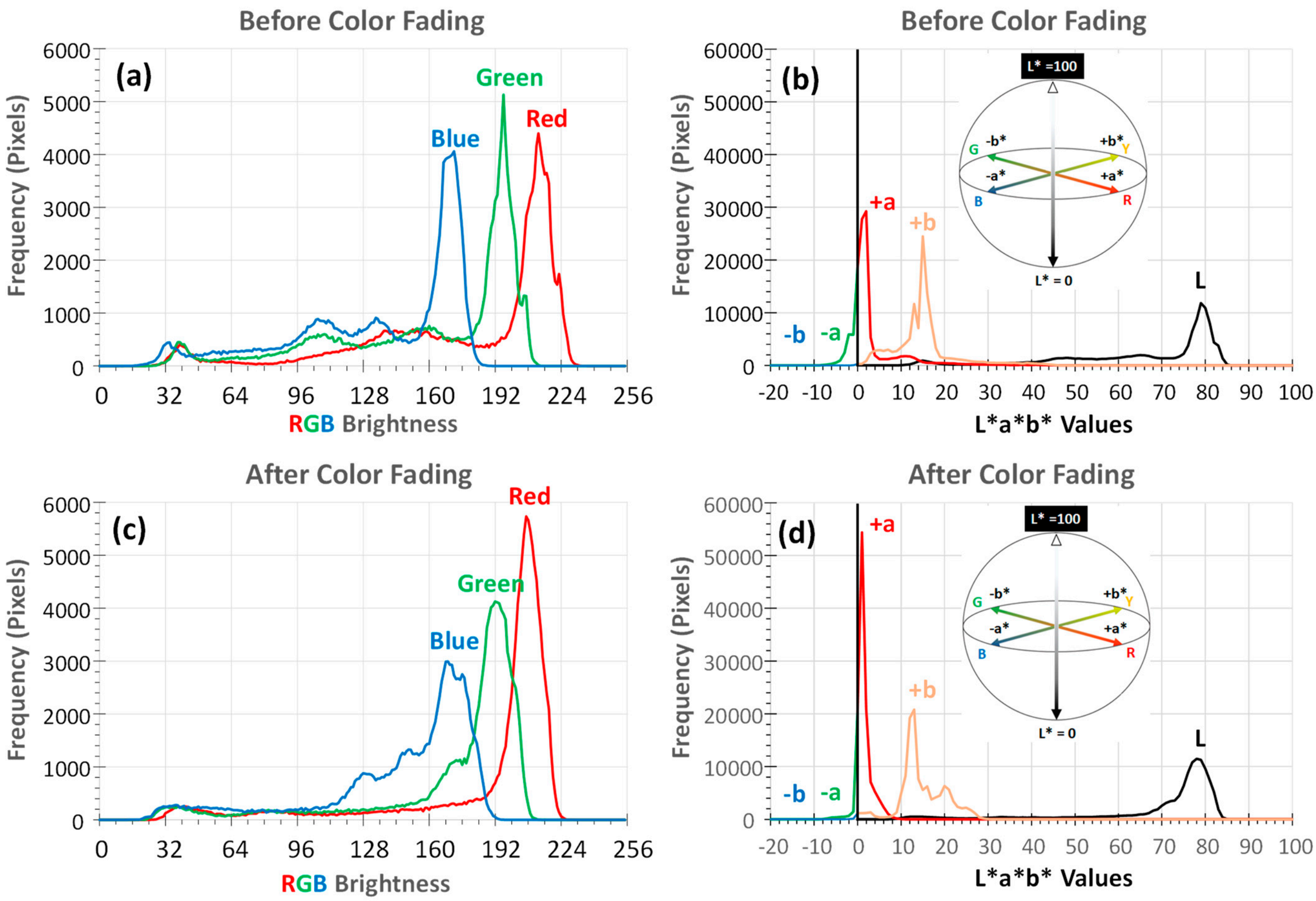

Figure 3. RGB and CIE L*a*b* histograms of a 284 × 422 pixel (=119,848 pixels) rectangle area per print: (**a**) RGB histogram of the original copy; (**b**) CIE L*a*b* histogram of the original copy; (**c**) RGB histogram of the faded copy; (**d**) CIE L*a*b* histogram of the faded copy.

Table 1. RGB and CIE L*a*b* statistics of a 284 × 422 pixel (= 119,848 pixels) rectangle area before and after color fading.

	Before Color Fading						After Color Fading					
	Red	**Green**	**Blue**	**L***	**a***	**b***	**Red**	**Green**	**Blue**	**L***	**a***	**b***
Count	119,848 Pixels						119,848 Pixels					
Minimum	18	22	10	7.7	−12.5	−5.4	21	13	10	4.9	−13.4	−8.3
Average	180.1	160.6	135.9	66.7	3.5	15.5	187.2	170.9	145.4	70.2	1.9	15.3
Maximum	242	215	190	86.4	51.5	52.9	231	219	199	87.8	15.3	33.6
Range	224	193	180	78.7	64.0	58.2	210	206	189	82.8	28.7	41.9
StdDev	47.2	46.0	41.2	17.7	6.6	7.2	44.4	41.6	38.8	16.6	1.9	5.4

3.2. Point-by-Point Color Extraction

Point-by-point color information was extracted from 34 points per image, as indicated in Figure 2. The identical locations on the two images, before and after color fading, were selected for color information extraction. The average colors of the five-pixel diameter circles were extracted and summarized in Table 2. Average RGB values, average HSV values, and average CIE L*a*b* values with average colors of 34 five-pixel diameter areas on the prints, before and after color fading (and darkening), are listed side-by-side for easy comparison.

Table 2. Average RGB values, average HSV values, average CIE L*a*b* values, and average colors of 34 five-pixel diameter areas at identical locations on the prints before and after color fading.

	Before Fading										After Fading									
No.	**R**	**G**	**B**	**H**	**S**	**V**	**L***	**a***	**b***	**Color**	**R**	**G**	**B**	**H**	**S**	**V**	**L***	**a***	**b***	**Color**
1	210	194	172	34.7	0.2	0.8	79.2	2.1	13.1		211	197	176	36.0	0.2	0.8	80.1	1.5	12.3	
2	181	153	95	40.5	0.5	0.7	64.5	2.7	34.2		187	173	151	36.7	0.2	0.7	71.3	1.4	13.1	
3	47	46	40	51.4	0.2	0.2	18.8	−0.9	4.0		49	47	43	40.0	0.1	0.2	19.5	0.0	2.9	
4	207	144	118	17.5	0.4	0.8	65.4	20.7	23.4		206	185	154	35.8	0.3	0.8	76.2	2.7	18.5	
5	200	175	116	42.1	0.4	0.8	72.4	0.9	33.5		207	190	156	40.0	0.3	0.8	77.6	0.7	19.4	
6	212	194	167	36.0	0.2	0.8	79.3	2.0	15.9		215	201	183	33.7	0.2	0.8	81.6	1.9	10.7	
7	181	155	96	41.6	0.5	0.7	65.1	1.7	34.4		179	162	136	36.3	0.2	0.7	67.4	2.0	15.8	
8	145	137	117	42.9	0.2	0.6	57.3	−0.5	11.8		172	156	133	35.4	0.2	0.7	65.2	2.1	14.2	
9	226	205	175	35.3	0.2	0.9	83.4	2.7	17.6		217	204	183	37.1	0.2	0.9	82.6	1.1	12.1	
10	216	198	171	36.0	0.2	0.9	80.7	2.0	15.8		210	194	171	35.4	0.2	0.8	79.2	1.9	13.6	
11	211	168	144	21.5	0.3	0.8	72.1	12.4	18.4		180	162	140	33.0	0.2	0.7	67.6	3.0	13.8	
12	218	201	171	38.3	0.2	0.9	81.6	1.2	17.2		213	197	176	34.1	0.2	0.8	80.3	2.2	12.6	
13	192	143	123	17.4	0.4	0.8	63.6	15.9	17.9		192	174	151	33.7	0.2	0.8	72.0	2.8	14.2	
14	209	157	134	18.4	0.4	0.8	69.0	16.3	19.6		208	185	154	34.4	0.3	0.8	76.3	3.4	18.8	
15	188	94	75	10.1	0.6	0.7	50.9	36.2	28.3		191	163	127	33.7	0.3	0.8	68.6	5.0	22.5	
16	157	154	134	52.2	0.2	0.6	63.3	−2.5	10.9		207	188	152	39.3	0.3	0.8	77.0	1.2	20.7	
17	161	159	141	54.0	0.1	0.6	65.2	−2.5	9.7		209	190	154	39.3	0.3	0.8	77.7	1.2	20.7	
18	215	198	167	38.8	0.2	0.8	80.5	1.1	17.7		207	189	162	36.0	0.2	0.8	77.4	2.1	16.0	
19	102	95	78	42.5	0.2	0.4	40.5	−0.3	10.8		140	129	110	38.0	0.2	0.6	54.5	0.9	11.8	
20	218	200	174	35.5	0.2	0.9	81.4	2.2	15.3		205	189	166	35.4	0.2	0.8	77.4	1.9	13.7	
21	117	88	64	27.2	0.5	0.5	39.8	8.6	18.5		94	89	66	49.3	0.3	0.4	37.7	−2.1	14.1	
22	201	176	126	40.0	0.4	0.8	72.9	1.9	28.9		193	176	142	40.0	0.3	0.8	72.5	0.8	19.7	
23	135	102	101	1.8	0.3	0.5	46.4	13.1	5.7		191	161	122	33.9	0.4	0.8	68.0	5.5	24.4	
24	125	96	78	23.0	0.4	0.5	43.2	9.1	14.8		122	110	81	42.4	0.3	0.5	46.8	−0.1	17.9	
25	139	104	98	8.8	0.3	0.6	47.3	13.1	8.8		190	158	115	34.4	0.4	0.8	67.0	5.8	26.9	
26	130	99	84	19.6	0.4	0.5	44.7	10.3	13.4		149	131	97	39.2	0.4	0.6	55.6	1.6	20.9	
27	190	175	151	36.9	0.2	0.8	72.1	1.5	14.3		180	164	141	35.4	0.2	0.7	68.2	2.1	14.1	
28	156	154	134	54.5	0.1	0.6	63.3	−2.9	10.8		206	186	150	38.6	0.3	0.8	76.3	1.6	20.9	
29	112	84	61	27.1	0.5	0.4	38.1	8.4	17.9		122	112	81	45.4	0.3	0.5	47.4	−1.2	18.7	
30	193	171	129	39.4	0.3	0.8	70.9	1.7	24.6		193	177	146	39.6	0.2	0.8	72.8	0.8	18.0	
31	205	137	111	16.6	0.5	0.8	63.4	23.0	24.5		183	156	121	33.9	0.3	0.7	65.9	4.8	22.1	
32	105	98	70	48.0	0.3	0.4	41.5	−2.0	17.0		131	122	92	46.2	0.3	0.5	51.3	−1.6	17.7	
33	205	155	127	21.5	0.4	0.8	68.0	14.9	21.9		207	186	152	37.1	0.3	0.8	76.5	2.2	20.0	
34	208	191	164	36.8	0.2	0.8	78.1	1.7	15.8		208	193	167	38.0	0.2	0.8	78.7	1.1	15.0	

All color information in a digital image file consists of a set of RGB intensity and pixel coordinate information. The RGB values can be translated into color values in other color space systems such as HSV, CIE L*a*b*, Munsell color, XYZ, and hexadecimal color codes. Table 2 shows HSV, CIE L*a*b*, and corresponding hexadecimal colors translated from RGB values of the images before and after color fading. As seen from the average colors for the 34 locations on the images, before and after color fading in Table 2, the majority of locations showed noticeable changes of colors after color fading (and darkening) by light illumination.

To make color differences before and after fading, the average colors at 34 locations were summarized in the order of $\Delta E_{L^*a^*b^*}$ (Table 3). The colors before and after color fading were shown side-by-side and provided differences in R, G, B, H, S, V, L*, a*, b*, and $\Delta E_{L^*a^*b^*}$. The color difference $\Delta E_{L^*a^*b^*}$ is defined as:

$$E_{L^*a^*b^*} = \sqrt{\left(L_1^* - L_2^*\right)^2 + \left(a_1^* - a_2^*\right)^2 + \left(b_1^* - b_2^*\right)^2} \tag{1}$$

where $\Delta E_{L^*a^*b^*} \approx 2.3$ (JND: a noticeable difference in the CIE76 formula. The $\Delta E_{L^*a^*b^*}$ values ranged from 1.2 to 36.3. Only three out of 34 locations have $\Delta E_{L^*a^*b^*} \approx 2.3$ (or JND) before and after color fading and color darkening. Background and hair colors were the only colors with negligible or unrecognizable fading. In other words, 31 out of 34 locations showed noticeable color differences.

Table 3. Difference between average RGB values, average HSV values, average CIE L*a*b* values, and their average colors of 34 five-pixel diameter areas at identical locations on the prints before and after color fading in the ascending order of $\Delta E_{L^*a^*b^*}$ rank.

		Color		Color Difference between before and after Fading (before—after)									
ΔE Rank	**No.**	**Before**	**After**	**ΔR**	**ΔG**	**ΔB**	**ΔH**	**ΔS**	**ΔV**	**ΔL***	**Δa***	**Δb***	$\Delta E_{L^*a^*b^*}$
1	34			0	−2	−3	−1.2	0.01	0	−0.6	0.62	0.8	1.2
2	1			−1	−3	−4	−1.3	0.01	−0.01	−0.9	0.6	0.81	1.4
3	3			−2	−1	−3	11.4	0.03	−0.01	−0.7	−0.89	1.15	1.6
4	10			6	4	0	0.6	0.02	0.03	1.5	0.13	2.22	2.7
5	18			8	9	5	2.8	0	0.03	3.1	−1	1.74	3.7
6	27			10	11	10	1.5	−0.01	0.04	3.9	−0.59	0.21	3.9
7	20			13	11	8	0.1	0.01	0.05	4	0.24	1.62	4.3
8	12			5	4	−5	4.2	0.05	0.01	1.3	−0.99	4.6	4.9
9	6			−3	−7	−16	2.3	0.06	−0.01	−2.3	0.14	5.15	5.6
10	9			9	1	−8	−1.8	0.07	0.04	0.8	1.61	5.53	5.8
11	30			0	−6	−17	−0.2	0.09	0	−1.9	0.92	6.61	6.9
12	8			−27	−19	−16	7.5	−0.04	−0.1	−7.9	−2.6	−2.38	8.7
13	22			8	0	−16	0	0.11	0.03	0.4	1.11	9.28	9.4
14	32			−26	−24	−22	1.8	0.03	−0.1	−9.8	−0.43	−0.73	9.8
15	24			3	−14	−3	−19.4	0.04	0.01	−3.6	9.15	−3.11	10.3
16	11			31	6	4	−11.5	0.1	0.12	4.5	9.38	4.56	11.4
17	21			23	−1	−2	−22.1	0.15	0.09	2.1	10.67	4.46	11.8
18	29			−10	−28	−20	−18.3	0.12	−0.04	−9.3	9.59	−0.75	13.4
19	19			−38	−34	−32	4.5	0.03	−0.15	−14	−1.19	−1.07	14.1
20	14			1	−28	−20	−16	0.1	0	−7.3	12.85	0.81	14.8
21	5			−7	−15	−40	2.1	0.17	−0.03	−5.2	0.2	14.17	15.1
22	33			−2	−31	−25	−15.6	0.11	−0.01	−8.5	12.7	1.94	15.4
23	26			−19	−32	−13	−19.6	0	−0.07	−10.9	8.69	−7.57	15.9
24	13			0	−31	−28	−16.3	0.15	0	−8.4	13.09	3.72	16.0
25	28			−50	−32	−16	15.9	−0.13	−0.2	−13	−4.43	−10.1	17.0
26	17			−48	−31	−13	14.7	−0.14	−0.19	−12.5	−3.67	−11	17.1
27	16			−50	−34	−18	12.9	−0.12	−0.19	−13.7	−3.64	−9.79	17.2
28	31			22	−19	−10	−17.3	0.12	0.08	−2.5	18.19	2.49	18.5
29	7			2	−7	−40	5.3	0.23	0.01	−2.3	−0.34	18.6	18.7
30	4			1	−41	−36	−18.3	0.18	0	−10.8	18.05	4.91	21.6
31	2			−6	−20	−56	3.8	0.29	−0.02	−6.8	1.27	21.11	22.2
32	25			−51	−54	−17	−25.6	−0.1	−0.2	−19.7	7.27	−18.1	27.7
33	23			−56	−59	−21	−32.1	−0.11	−0.22	−21.6	7.65	−18.7	29.6
34	15			−3	−69	−52	−23.6	0.26	−0.01	−17.7	31.17	5.76	36.3

Figure 4 shows the RGB value change before and after fading and their colors at 34 five-pixel diameter ROIs in the ascending order of CIE $\Delta E_{L^*a^*b^*}$ rank, from left to right. Thick colored lines and thin black lines are the intensity (or brightness) of each color channel before and after color fading. Color fading generally makes the intensity (or brightness) increase in all RGB color channels except for a few measurement locations indicated with arrows. It clearly indicates that most colors become lighter after color fading. However, a few colors became darker under light illumination, as seen in the locations with negative CIE ΔL* values in Table 3. The red and green channel intensity changed noticeably compared to the blue channel intensity after color fading by light illumination. In general, darker colors with lower red and green intensities tend to fade more and result in noticeable color changes. As the results changed in the CIE, $\Delta E_{L^*a^*b^*}\Delta$ was higher for the darker colors.

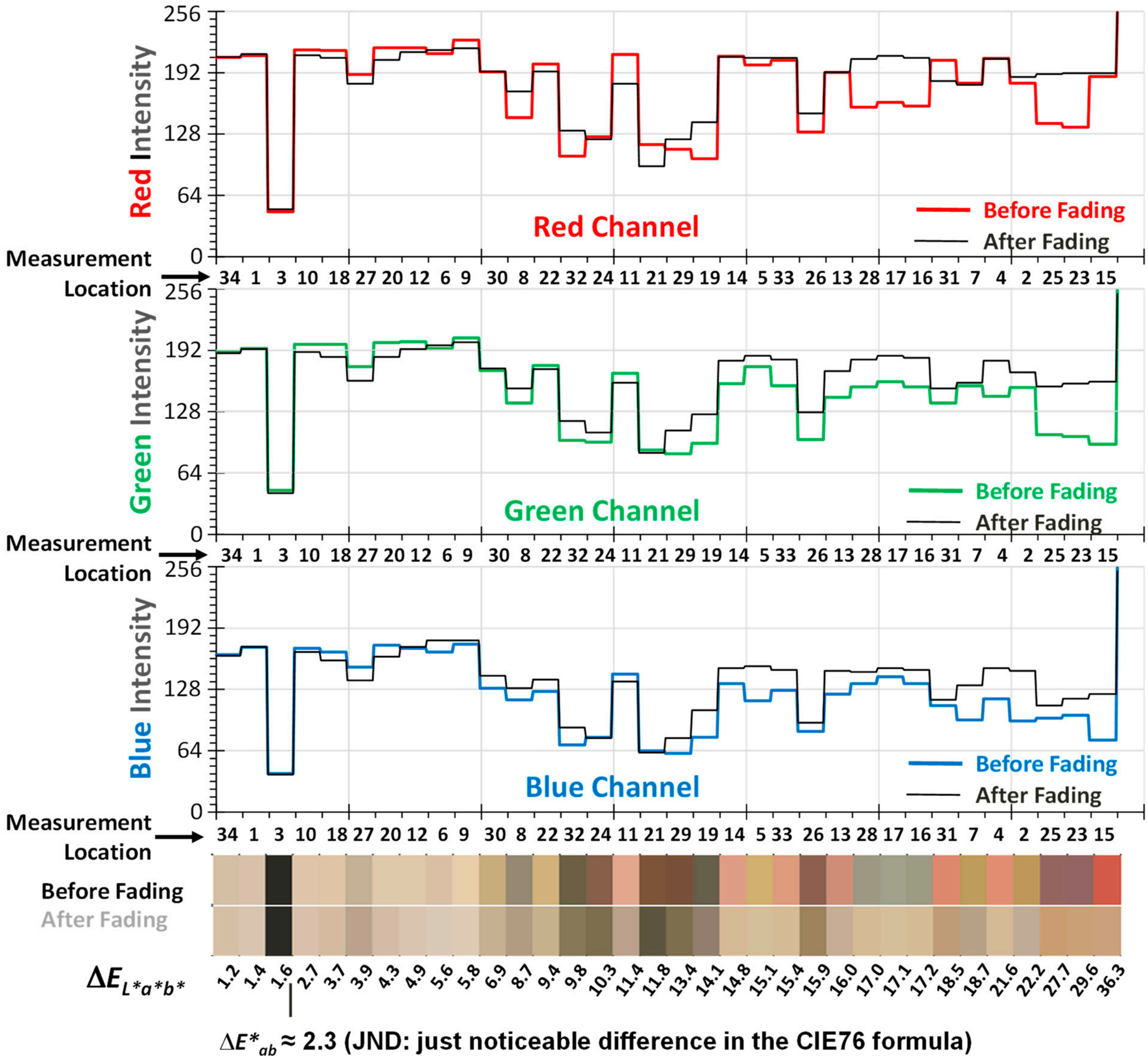

Figure 4. RGB value change before and after fading and their colors at 34 five-pixel diameter ROIs in the ascending order of CIE $\Delta E_{L^*a^*b^*}$ rank, from left to right.

3.3. Line-by-Line Color Extraction

Line-by-line color information was extracted from 10 lines, as shown in Figure 5. Color information can be extracted from all lines in any direction, including free lines. Figure 6 shows the RGB intensity profile along 4 selected lines 2, 6, 8, and 10. Colors of a few locations per line showing noticeable color differences before and after color fading were shown together with RGB intensity line graphs.

Similar trends for color change by color fading, summarized in Tables 2 and 3, can be verified in Figure 6. Average RGB values and their ranges are very different between the two copies of the prints, before and after color fading. The average RGB value for the original copy of the print is smaller than the color faded copy. The RGB intensity range for the original copy of the print is much wider due to the large contrast of colors along the horizontal lines 6, 8, and 10. In contrast, the color-faded copy of the print shows a narrower range of RGB intensity values.

All colors can be quantified as RGB, HSV, CIE L*a*b*, XYZ, and Munsell color values, even with hexadecimal color codes. The extracted color information can be graphed for objective evaluation. Discoloration (or color fading) rate can be quantitatively determined per colorant as a function of the light exposure conditions. The MFT results can also be characterized by digital photography and used as a color fading database for individual colorants.

(**a**) (**b**)

Figure 5. Ten numbered lines for color extraction and comparison between two identical copies of a Japanese woodblock print by Japanese artist Utamaro before and after significant light exposure: (**a**) as printed; (**b**) after light exposure.

3.4. Pixel-by-Pixel Image Comparison

Figure 7 shows a summary of the pixel-by-pixel image comparisons of the two copies of a print before and after color fading. For the alignment of two images, we overlapped the two images and translated one image in x and y coordinates pixel-by-pixel to minimize the color difference due to the misalignment. In fact, we found that the two images were digitized in the same magnification, and only two pixels in the y coordinate were off between the two images. Thus, the two images were suitable for pixel-by-pixel color comparisons. The pixel-by-pixel color differences were mapped in terms of the CIE ΔL*, CIE Δa*, CIE Δb*, and CIE ΔE* values at full scale (100% scale) and at quarter scale (25% of full scale) for easy recognition of changes by color fading. The full-scale images are shown in the top row, and the quarter-scale images are shown in the bottom row. Since the color differences along the CIE a* and CIE b* axes were small compared to the lightness of the CIE L* axis, the full-scale pixel-by-pixel color difference mapping images for the CIE Δa* and CIE Δb* values did not show significant color differences. The light exposure induced color differences in lightness in CIE ΔL*, color shift (in CIE Δa* and CIE Δb*), and color difference in CIE ΔE* were four (4) times magnified in quarter scale images.

The CIE L*a*b* color space expresses color as three values. The lightness value CIE L* defines black as 0 and white as 100. The CIE a* axis is relative to the green–red opponent colors, green (negative CIE a* values) to red (positive CIE a* value). The b* axis is relative to the blue–yellow opponent colors, blue (negative CIE b* values) to yellow (positive CIE b* value). The CIE a* and CIE b* axes are independent in the range of −128 to 127. In CIE L*a*b* color space, CIE L* is for perceptual lightness, and CIE a* and CIE b* are for the four unique colors of human vision, red, green, blue, and yellow. The CIE ΔL* and CIE ΔE* values are in grayscale because they only have a magnitude in the brightness and overall color difference. The CIE Δa* and CIE Δb* values can be negative, zero (i.e., no color difference along the CIE a* axis for red and green balance or CIE b* axis for yellow and blue balance), or positive.

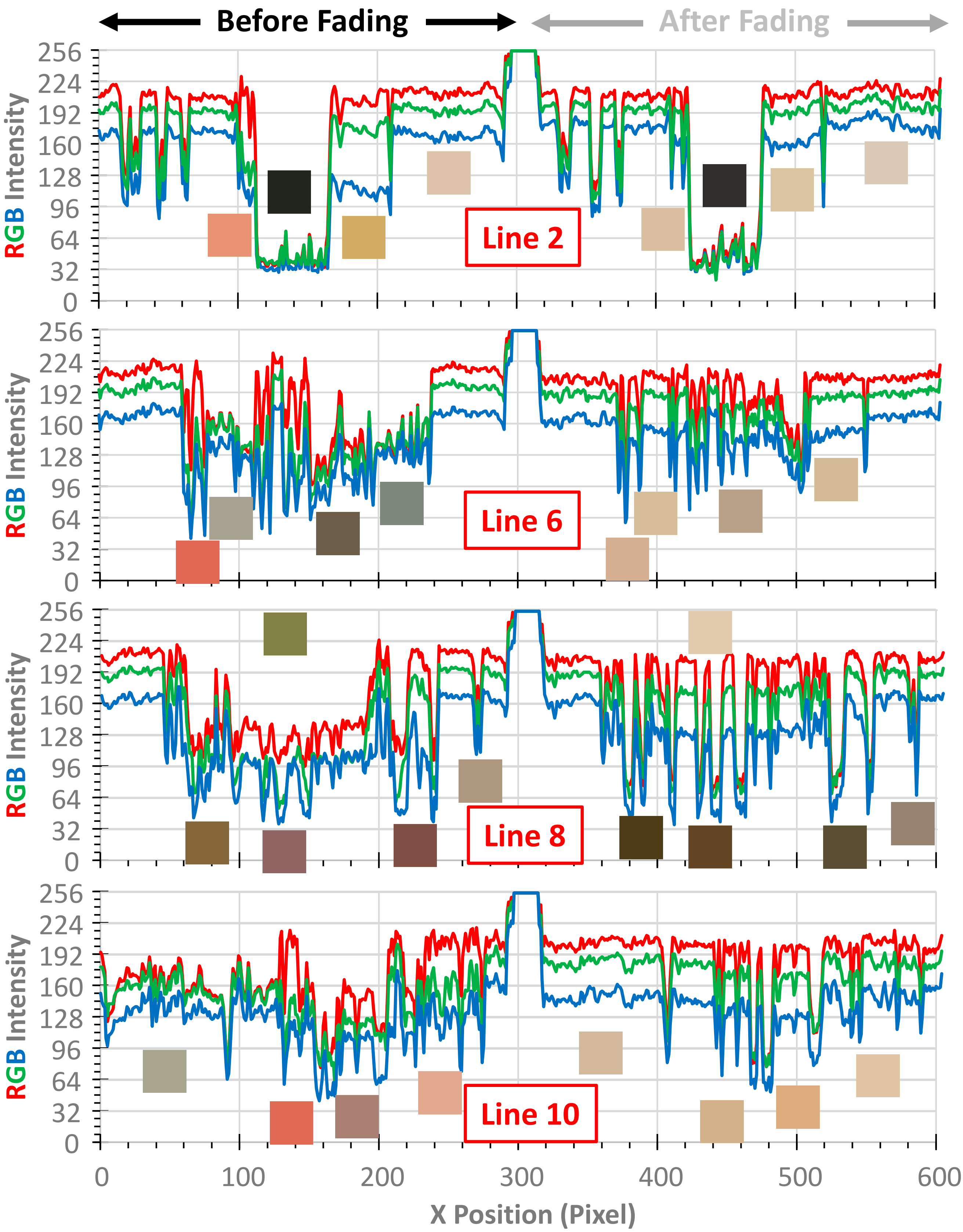

Figure 6. RGB values change across lines 2, 6, 8, and 10 on the image on the left. Colors of sections of noticeable color change before and after light illumination are shown for easier recognition and interpretation of RGB values.

The degrees of the color shifts along the CIE a* and CIE b* axes can be easily recognized, pixel by pixel, from Figure 7. The color difference CIE ΔE* can easily be determined and visualized pixel by pixel. This type of detailed pixel-by-pixel color difference characterization cannot be measured or visualized by conventional chroma meter measurements due to spatial resolution limits [19–21,28,29].

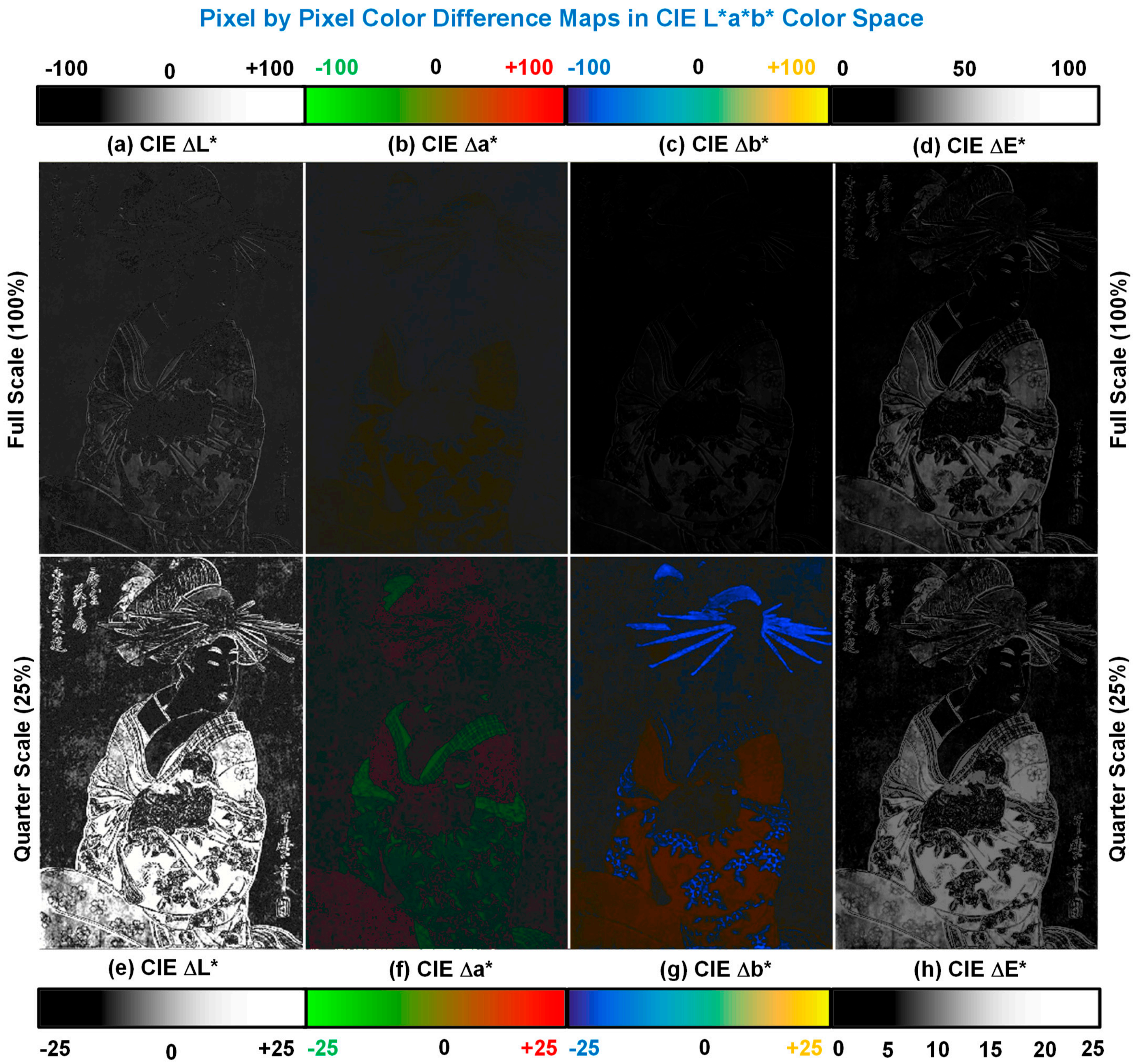

Figure 7. Pixel-by-pixel color difference in images in full scale (top row) and quarter scale (4× zoomed scale or 25% of full scale) (bottom row); (**a**) ΔL*; (**b**) Δa*; (**c**) Db*; (**d**) DE* in full scale; (**e**) DL*; (**f**) Δa*; (**g**) Δb*; (**h**) ΔE* in quarter scale (4× zoomed scale or 25% of full scale). Legends are given for easy recognition of pixel-by-pixel brightness, color shift, and color difference.

3.5. Block-by-Block Image Comparison

The two copies of a print, before and after color fading, were compared block-by-block using image processing/analysis software (PicMan). The block size was varied from 20 × 20 pixels to 50 × 50 pixels in 10-pixel increments (Figure 8). Upper-left and lower-right triangles show partial images before and after color fading for an easy comparison of the effect of color fading within areas of the same color patterns. The block-by-block image comparison technique, by alternating partial masking of the two comparing images with changing block size, provides intuitive synthesized images for side-by-side comparison on the reference image.

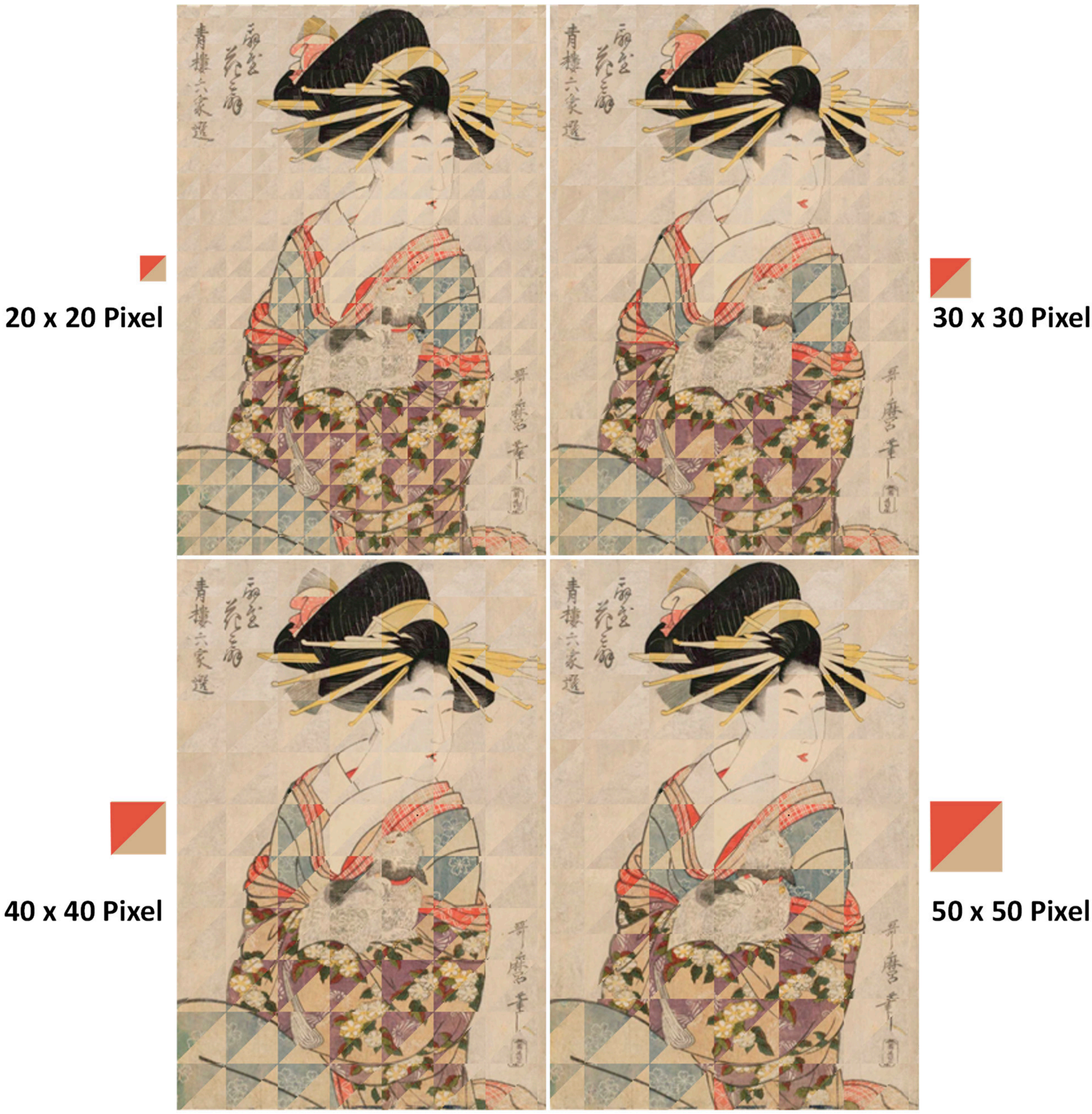

Figure 8. Block-by-block comparison images (top left triangle for the original image and bottom right triangle for color faded image) with four different block sizes of 20 × 20 pixel, 30 × 30 pixel, 40 × 40 pixel, and 50 × 50 pixel squared blocks.

The actual area of measurement can be calculated by the scale of an image in pixel/mm. The scale of an image can be easily calculated by measuring the actual dimensions of the print in mm and the size of the image in pixels. The image resolution of the scale is expressed in pixels/mm.

Background colors became darker after color fading by light exposure. The color difference in black hair and wig areas was hard to recognize by visual inspection due to their very low brightness (i.e., very low RGB values, low CIE L* value, low V value in a HSV color space). The red, pink, yellow, bluish, and purple colored areas showed noticeable color fading. The purple-colored area showed the most discoloration. The red, pink, and bluish-colored areas also had undergone significant discoloration and transformed into almost similar colors, as seen in Figures 1 and 8.

While the point-by-point, line-by-line, and area-by-area color characterization techniques are useful for quantifying color differences between two images, the block-by-block color comparison provides visual instinct on color differences between images at the desired block size.

3.6. Color Simulation by Interpretation and Extrapolation

In theory, if images of identical objects from different times are available, new images can be generated by image blending and/or image morphing. It is very similar to the interpolation between data sets acquired from two different times. The micro fading test data for discoloration under controlled light exposure conditions can be used as important data points for understanding color fading phenomena and mechanisms. If color extrapolation beyond the two data points is feasible, simulated images outside of the time frame for the two images can be generated.

Figure 9 shows image blending simulation results using two true images by interpolation. Figure 9a,b is the original image at time A, and the color faded image at time B. Figure 9c is the interpolated result image for color fading in progress in the middle of times A and B. The image was generated by 50:50 blending or interpolation of the two images. By changing the blending ratio, many simulated images can be generated at different times between times A and B, as shown in Figure 10. Furthermore, extrapolation can be done before time A and beyond time B assuming the rate of color change are constant.

(**a**) (**b**) (**c**)

Figure 9. Demonstration of image blending simulation using two true images by interpolation; (**a**) original image at time A; (**b**) interpolated image for color fading in progress; (**c**) fully faded image at time B.

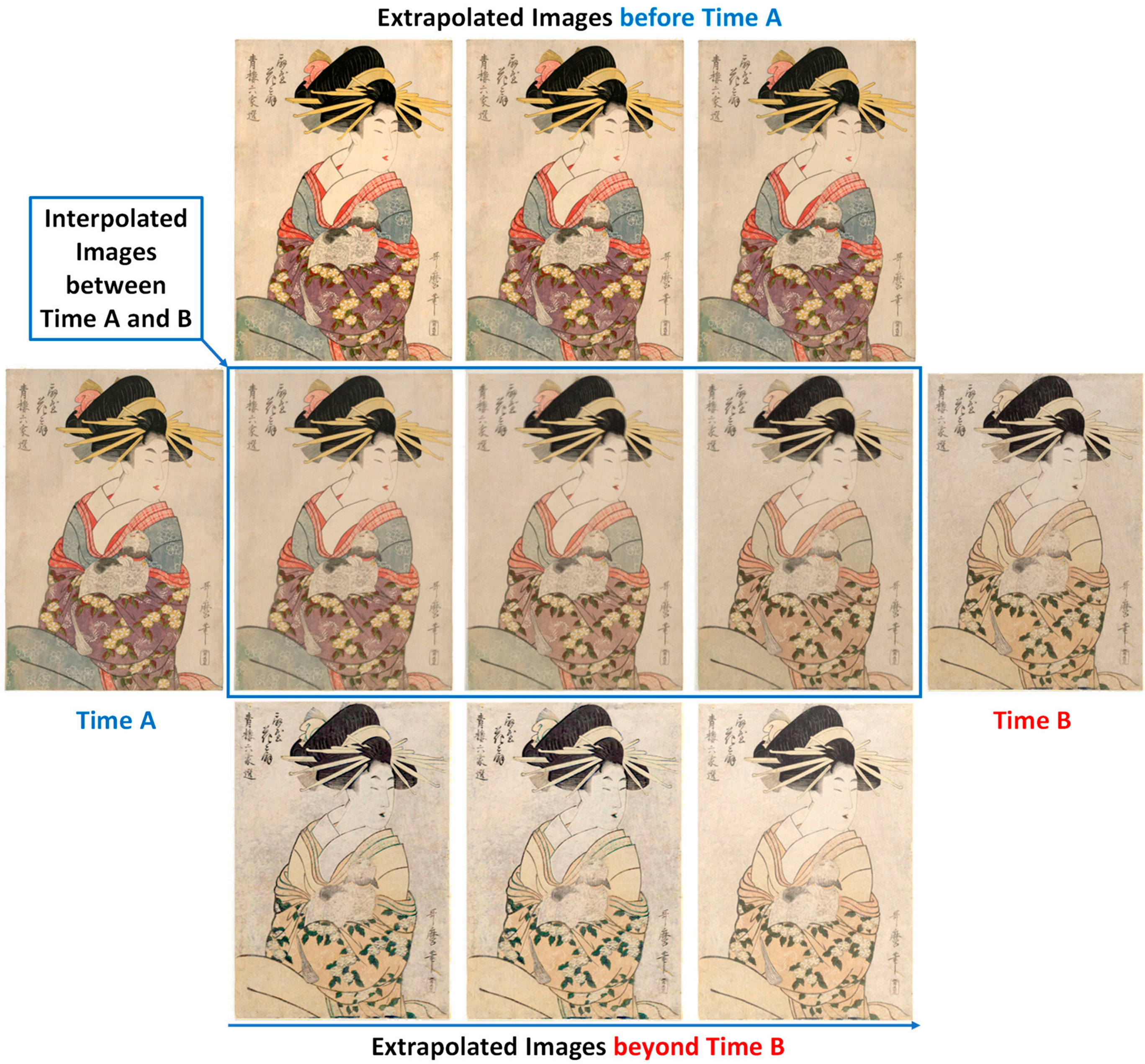

Figure 10. Demonstration of extrapolated images and interpolated images based on two images at time A (at the time of printing, before color fading occurs or any reference point of time) and B (at any point of time after time A for color comparison).

In the real world, the rate of color change of each colorant is neither linear nor infinite. The purpose of this paper is to demonstrate possible color change simulations using a simple color change model under a given light illumination condition. When the color change rate of individual colorants at a given illumination and time condition is characterized, a real color change rate can be applied for color change simulations for a realistic effect.

3.7. Potential Applications

Diagnoses of the conservation status of painting cultural heritages and color fading characteristics of pigments using this quantitative colorimetric analysis technique were also very promising [19–21]. It has been extremely useful for digital forensic studies of cultural heritage identification processes. In particular, printing techniques of ancient Korean books through ink tone analyses and character image comparisons with images of books with known printing techniques and printing dates [30–33]. Darkening by oxidation of *Hanji* (Korean paper) used in the ancient books was removed from photographed images for unbiased ink tone analysis and fair comparison between several versions of nearly identical ancient books. This led to the discovery of the world's oldest metal-type printed book (*The Song of Enlightenment* (南明泉和尚頌證道歌) in Korea in 1239). The world's oldest metal-type printed book from the Goryeo dynasty of Korea, from the 13th century, has been identified by comparing six nearly identical books from Korea from the 13th to 16th centuries, the *Jikji* (直指) printed in 1377 and the Gutenberg 42-line Bible, printed in 1455 using this quantitative image analysis technique [34]. Many other applications based on color/shape extraction and area measurement techniques using the newly developed image processing/analysis software (PicMan) are expanding. Image processing software applications combined with imaging devices such as USB cameras and professional digital cameras have been reported in previous papers [19–24].

4. Summary

Quantitative characterization of color from images is very important in the fields of color-related applications. In the fields of art, cultural heritage, and museum, color fading and color darkening under light exposure is one of many important and unavoidable natural processes. Color naturally fades with time under light illumination in an oxidizing environment. If the chemical environment of storage is altered, the color may fade or darken abnormally. Quantitative characterization of colors becomes very important, regardless of the conventional colorimetric approach or photometric approach. In this paper, a novel approach to the quantitative characterization of color and visualization of color fading and color darkening, using a newly developed image analysis and comparison software (PicMan), is proposed and demonstrated.

The rate of color fading depends on the substance, lighting condition, and chemical environment of storing facilities. Color fading is only observed as a result after the damage is done. The current color of objects of interest can only be compared with old photographs or the observer's perceived memory at the time of reference. There is no guarantee that the same individual will inspect or properly evaluate the color change. Color difference and color fading rate between two or more points of time in the past can only be determined using photographic images from the past unless the other colorimetric measurements were made at the time of inspection.

Quantification of color in either digital or printed photographs is required for objective characterization of color differences between two or more different times. Image analysis and comparison software-assisted color quantification and pixel-by-pixel color difference mapping were proposed and demonstrated in this study. Images of two copies of Japanese woodblock prints, with and without color fading, have been selected for exemplary study. Pixel-by-pixel, line-by-line, area-by-area, and block-by-block comparisons of color fading between two images were found to be very effective in the quantification of color fading and visualization of the phenomena. RGB, HSV, CIE L*a*b* values between images and the differences of single pixels to areas of interest in any shape and size can be quantified and exported as numerical and traceable data.

Color fading and color darkening analysis results were presented in numerical, graphical, and image formats for completeness. As demonstrated in this study, all formats have their own advantages and disadvantages over other formats in terms of data size, complexity, readability, and communication among parties of interest. Various display options for color analysis summary of color fading and color darkening were demonstrated using the images of interest for practical artistic, cultural heritage conservation, and museum applications. Color simulation for various moments in time was proposed and demonstrated by interpolation or extrapolation of color change between images, with and without color fading, using PicMan. The degree of color fading and color darkening in the various moments in the past and future can be simulated and visualized for decision-making in public display, storage, and restoration planning.

Author Contributions: All authors equally contributed to this study. Conceptualization, W.S.Y., K.K. and Y.Y.; material preparation, W.S.Y. and Y.Y.; methodology, Y.Y. and J.G.K.; software, W.S.Y. and K.K.; data acquisition and analysis, Y.Y., J.G.K. and W.S.Y.; writing—original draft preparation, review and editing, W.S.Y. and Y.Y. All authors have read and agreed to the published version of the manuscript.

Funding: This research received no external funding.

Conflicts of Interest: The authors declare no conflict of interest.

References

1. Special Post–Microfading Workshop! Available online: https://intheirtruecolors.wordpress.com/2014/09/26/special-post-microfading-workshop/ (accessed on 30 April 2023).
2. Van Gogh's Fading Colors Inspire Scientific Inquiry. Available online: https://cen.acs.org/articles/94/i5/Van-Goghs-Fading-Colors-Inspire.html (accessed on 30 April 2023).
3. Hofmann, M.; Hofmann-Sievert, R. Spectral Light Fading of Inkjet Prints. *Heritage* **2022**, *5*, 4061–4073. [CrossRef]
4. NASA Science, Tour of the Electromagnetic Spectrum. Available online: https://science.nasa.gov/ems/09_visiblelight#:~:text=Typically%2C%20the%20human%20eye%20can,from%20380%20to%20700%20nanometers (accessed on 30 April 2023).
5. Zhao, Y.; Wang, J.; Pan, A.; He, L.; Simon, S. Degradation of red lead pigment in the oil painting during UV aging. *Color Res. Appl.* **2019**, *44*, 790–797. [CrossRef]
6. Beltran, V.L.; Pesme, C.; Freeman, S.K.; Benson, M. *Microfading Tester: Light Sensitivity Assessment and Role in Lighting Policy Guidelines*; Getty Conservation Institute: Los Angeles, CA, USA, 2021; Available online: https://www.getty.edu/conservation/publications_resources/pdf_publications/pdf/Microfading_Tester.pdf (accessed on 30 April 2023).
7. Whitmore, P.M.; Pan, X.; Bailie, C. Predicting the Fading of Objects: Identification of Fugitive Colorants through Direct Nondestructive Lightfastness Measurements. *J. Am. Inst. Conserv.* **1999**, *38*, 395–409. [CrossRef]
8. Fieberg, J.E.; Knutås, P.; Hostettler, K.; Smith, G.D. "Paintings Fade Like Flowers": Pigment Analysis and Digital Reconstruction of a Faded Pink Lake Pigment in Vincent van Gogh's Undergrowth with Two Figures. *Appl. Spectrosc.* **2017**, *71*, 794–808. [CrossRef] [PubMed]
9. Amanatiadis, S.; Apostolidis, G.; Karagiannis, G. Consistent Characterization of Color Degradation Due to Artificial Aging Procedures at Popular Pigments of Byzantine Iconography. *Minerals* **2021**, *11*, 782. [CrossRef]
10. Eickhoff, A.J.; Hunter, R.S.; Measurement of the Fading Rate of Paints. RESEARCH PAPER RP1478, Part of Journal of Research of the National Bureau of Standards, Volume 28, June 1942. Available online: https://nvlpubs.nist.gov/nistpubs/jres/28/jresv28n6p773_A1b.pdf (accessed on 30 April 2023).
11. Kirby, J.; Saunders, D. 'Fading and Colour Change of Prussian Blue: Methods of Manufacture and the Influence of Extenders'. *Natl. Gallery Tech. Bull.* **2004**, *25*, 73–99. Available online: http://www.nationalgallery.org.uk/technical-bulletin/kirby_saunders2004 (accessed on 30 April 2023).
12. Melo, M.J.; Nabais, P.; Vieira, M.; Araújo, R.; Otero, V.; Lopes, J.; Martín, L. Between past and future: Advanced studies of ancient colours to safeguard cultural heritage and new sustainable applications. *Dye. Pigment.* **2022**, *208*, 110815. [CrossRef]
13. Zheng, L.; Wang, Z.; Shen, S.; Xia, Y.; Li, Y.; Hu, D. Blurring of ancient wall paintings caused by binder decay in the pigment layer. *Sci Rep.* **2020**, *10*, 21075. [CrossRef] [PubMed]
14. Kubik, M.A. Preserving the Painted Image: The Art and Science of Conservation. *Color Des. Creat.* **2010**, *5*, 1–8.
15. Lee, H.S.; Coates, G.A. Characterization of Color Fade during Frozen Storage of Red Grapefruit Juice Concentrates. *J. Agric. Food Chem.* **2002**, *50*, 3988–3991. [CrossRef] [PubMed]
16. Xia, Y.; Song, X.; Jia, Z.; Wang, X. Mechanism and quantitative characterization of color fading phenomenon of HTV composite insulators silicone rubber. In Proceedings of the 2018 12th International Conference on the Properties and Applications of Dielectric Materials (ICPADM) 2018, Xi'an, China, 20–24 May 2018. [CrossRef]
17. CSN EN 15886; Conservation of Cultural Property-Test Methods-Colour Measurement of Surfaces. CEN: Brussels, Belgium, 2010. Available online: https://www.en-standard.eu/csn-en-15886-conservation-of-cultural-property-test-methods-colour-measurement-of-surfaces/ (accessed on 31 July 2023).
18. Two Copies of a Japanese Woodblock Print by Utamaro. Available online: https://intheirtruecolors.files.wordpress.com/2014/09/fadeexample_woodblock.png (accessed on 30 April 2023).
19. Kim, G.; Kim, J.G.; Kang, K.; Yoo, W.S. Image-Based Quantitative Analysis of Foxing Stains on Old Printed Paper Documents. *Heritage* **2019**, *2*, 2665–2677. [CrossRef]
20. Yoo, W.S.; Kang, K.; Kim, J.G.; Yoo, Y. Extraction of Color Information and Visualization of Color Differences between Digital Images through Pixel-by-Pixel Color-Difference Mapping. *Heritage* **2022**, *5*, 3923–3945. [CrossRef]
21. Eom, T.H.; Lee, H.S. A Study on the Diagnosis Technology for Conservation Status of Painting Cultural Heritage Using Digital Image Analysis Program. *Heritage* **2023**, *6*, 1839–1855. [CrossRef]
22. Wakamoto, K.; Otsuka, T.; Nakahara, K.; Namazu, T. Degradation Mechanism of Pressure-Assisted Sintered Silver by Thermal Shock Test. *Energies* **2021**, *14*, 5532. [CrossRef]

23. Jo, S.-I.; Jeong, G.-H. Single-Walled Carbon Nanotube Synthesis Yield Variation in a Horizontal Chemical Vapor Deposition Reactor. *Nanomaterials* **2021**, *11*, 3293. [CrossRef] [PubMed]
24. Zhu, C.; Espulgar, W.V.; Yoo, W.S.; Koyama, S.; Dou, X.; Kumanogoh, A.; Tamiya, E.; Takamatsu, H.; Saito, M. Single Cell Receptor Analysis Aided by a Centrifugal Microfluidic Device for Immune Cells Profiling. *Bull. Chem. Soc. Jpn.* **2019**, *92*, 1834–1839. [CrossRef]
25. PicManTV. Available online: https://www.youtube.com/@picman-TV (accessed on 30 April 2023).
26. Kruschwitz, J.D.T. *Field Guide to Colorimetry and Fundamental Color Modeling*; SPIE Press: Washington, DC, USA, 2018.
27. Von Goethe, J.F. *Theory of Colours*; The MIT Press: Cambridge, MA, USA, 1970.
28. Rhyne, T.-M. *Applying Color Theory to Digital Media and Visualization*, 1st ed.; Association for Computing Machinery: New York, NY, USA, 2016.
29. Minolta, K. CR-400 Chroma Meter. Available online: https://sensing.konicaminolta.us/us/products/cr-400-chroma-meter-colorimeter/ (accessed on 30 April 2023).
30. Yoo, W.S. The World's Oldest Book Printed by Movable Metal Type in Korea in 1239: The Song of Enlightenment. *Heritage* **2022**, *5*, 1089–1119. [CrossRef]
31. Yoo, W.S. How Was the World's Oldest Metal-Type-Printed Book (The Song of Enlightenment, Korea, 1239) Misidentified for Nearly 50 Years? *Heritage* **2022**, *5*, 1779–1804. [CrossRef]
32. Yoo, W.S. Direct Evidence of Metal Type Printing in The Song of Enlightenment, Korea, 1239. *Heritage* **2022**, *5*, 3329–3358. [CrossRef]
33. Yoo, W.S. Ink Tone Analysis of Printed Character Images towards Identification of Medieval Korean Printing Technique: The Song of Enlightenment (1239), the Jikji (1377) and the Gutenberg Bible (~1455). *Heritage* **2023**, *6*, 2559–2581. [CrossRef]
34. American Printing History Association. History of Printing Timeline. Available online: https://printinghistory.org/timeline/ (accessed on 30 April 2023).